

Article

# Development of a Time-Gated Epithermal Neutron Spectrometer for Resonance Absorption Measurements Driven by a High-Intensity Laser

Zechen Lan <sup>1</sup>, Yasunobu Arikawa <sup>1</sup>, Yuki Abe <sup>2</sup>, Seyed Reza Mirfayzi <sup>3</sup>, Alessio Morace <sup>1</sup>, Takehito Hayakawa <sup>4</sup>, Tianyun Wei <sup>1</sup> and Akifumi Yogo <sup>1,\*</sup><sup>1</sup> Institute of Laser Engineering, Osaka University, Osaka 565-0871, Japan<sup>2</sup> Graduate School of Engineering, Osaka University, Osaka 565-0871, Japan<sup>3</sup> Tokamak Energy Ltd., Oxford OX14 4SD, UK<sup>4</sup> Kansai Institute for Photon Science, National Institute for Quantum Science and Technology, Kyoto 619-0215, Japan

\* Correspondence: yogo.akifumi.ile@osaka-u.ac.jp

**Abstract:** The advance of laser-driven neutron sources (LDNSs) has enabled neutron resonance spectroscopy to be performed with a single shot of a laser. In this study, we describe a detection system of epithermal ( $\sim$ eV) neutrons especially designed for neutron resonance spectroscopy. A time-gated photomultiplier tube (PMT) with a high cut-off ratio was introduced for epithermal neutron detection in a high-power laser experiment at the Institute of Laser Engineering, Osaka University. We successfully reduced the PMT response to the intense hard X-ray generated as a result of the interaction between laser light and the target material. A time-gated circuit was designed to turn off the response of the PMT during the laser pulse and resume recording the signal when neutrons arrive. The time-gated PMT was coupled with a  $^6\text{Li}$  glass scintillator, serving as a time-of-flight (TOF) detector to measure the neutron resonance absorption values of  $^{182}\text{W}$  and  $^{109}\text{Ag}$  in a laser-driven epithermal neutron generation experiment. The neutron resonance peaks at 4.15 eV of  $^{182}\text{W}$  and 5.19 eV of  $^{109}\text{Ag}$  were detected after a single pulse of laser at a distance of 1.07 m.

**Keywords:** experimental instruments; neutron spectrometer; laser plasma experiment; laser-driven neutron source; neutron resonance spectroscopy



**Citation:** Lan, Z.; Arikawa, Y.; Abe, Y.; Mirfayzi, S.R.; Morace, A.; Hayakawa, T.; Wei, T.; Yogo, A. Development of a Time-Gated Epithermal Neutron Spectrometer for Resonance Absorption Measurements Driven by a High-Intensity Laser. *Quantum Beam Sci.* **2024**, *8*, 9. <https://doi.org/10.3390/qubs8010009>

Academic Editor: Heloisa N. Bordallo

Received: 28 December 2023

Revised: 26 February 2024

Accepted: 27 February 2024

Published: 29 February 2024



**Copyright:** © 2024 by the authors. Licensee MDPI, Basel, Switzerland. This article is an open access article distributed under the terms and conditions of the Creative Commons Attribution (CC BY) license (<https://creativecommons.org/licenses/by/4.0/>).

## 1. Introduction

As newly developed tools for neutron generation, laser-driven neutron sources (LDNSs) have shown excellent potential in various fields, such as medicine [1], nuclear physics [2,3], inspection of materials [4], and industrial applications [5]. Some efficient methods of neutron generation using laser pulses, such as using high-energy ions (protons or deuterons) accelerated by laser-matter interactions to generate neutrons by nuclear reactions with a secondary target (Li or Be) [6,7], nuclear fusion [8], and photonuclear reactions [9,10], have been reported. Many theoretical and experimental attempts have been made to interpret the mechanism of ion acceleration resulting from the interaction between laser light and materials [11–15]. By focusing a laser beam on a thin foil target with a relativistic intensity, which exceeds  $10^{18} \text{ W}\cdot\text{cm}^{-2}$  for a wavelength of  $1 \mu\text{m}$ , electrons are accelerated toward the target's rear side and an intense electrical field is induced on the rear surface. The electrical field accelerates the ions towards the normal direction of the target's rear surface with an energy of up to several dozen MeV [16]. To achieve neutron generation, high-energy ions bombard the secondary target of Be and induce nuclear reactions of  $^9\text{Be}(p,n)^9\text{B}$  and  $^9\text{Be}(d,n)^{10}\text{B}$  to generate fast neutrons with energies of up to dozens of MeV and a quantity of  $10^{10} \text{ n/sr}$  [7,8,17,18]. The energy of these fast neutrons can be decreased by adding a moderator material, so some applications requiring cold, thermal, or epithermal neutron beams can be attempted with an LDNS [3,7,19,20].

Neutrons are generally measured by the time-of-flight (TOF) method [21], in which neutron signals are recorded temporally, and the energy is calculated from the flight speed. In high-energy laser-driven neutron experiments, one of the major hindrances to neutron measurement is that all reactions, including laser-induced ion acceleration and neutron generation, release a large amount of energy in the form of intense hard X-rays [5]. In most types of neutron TOF spectroscopy, a scintillation detector coupled with a photomultiplier tube (PMT) is typically used to record the fluorescence induced by neutrons. In fast neutron (with an energy of dozens of MeV) measurement, relatively long flight passes up to a few dozen meters have been used to provide a long flight time that keeps the neutron signal separated from the X-ray peak [7,17,18,22]. Although the intense X-ray generated by the laser shot could be separated from epithermal neutrons, the residual emissions in the scintillation crystals are still strong enough to overshadow the signals of the neutrons. In addition, with a long-time window of epithermal neutron measurement, a large amount of signal can saturate the PMT, leading to a loss of linearity in subsequent responses. When the distance of the TOF is longer, it is possible to separate a laser shot X-ray and neutron signals. Nevertheless, such longer TOF distance leads to fewer detected neutrons due to the quasi-isotropic generation of a laser-driven neutron source. To obtain good statistics and neutron utilization efficiency, a shorter distance is expected. However, the intensity of X-rays also increases when the detector is closer to the source. Therefore, there is a necessary requirement to cut off the X-ray signal.

To cut off the X-ray signal, some time-gated neutron detectors have been developed [23–25] for neutron detection. A customized electrical time-gating (ETG) system has been coupled with a PMT to stop the multiplication of electrons during a specific period by applying a reverse bias on the dynodes of the PMT [26–29]. Although PMTs with ETG systems have been developed for a long time and there are commercial modules providing ETG functions, few products are suitable for high-energy laser-driven neutron experiments. The overload current of the X-ray signal usually disables the commercial ETG circuit. Furthermore, there is another problem. Most models available for sale provide only relatively small photosensitive surfaces ( $\phi < 1$  cm), while detecting laser-driven neutrons requires large scintillators ( $\phi > 2$  cm). Therefore, commercial modules are not feasible for laser-driven neutron experiments.

For a time-gated PMT with an ETG system, the bias voltage is generally delivered by a capacitor. The charging time of the capacitor determines the speed of the switch. However, for high-energy laser experiments, the capacitor may be completely discharged in several to dozens of  $\mu\text{s}$ , causing the ETG to shut down earlier than the set time. As reported in [25], a high-speed ETG can provide a switching time of less than 100 ns by using a 10 nF capacitor (C2 in Ref. [25]). This design enables the detection of fast neutrons in high-energy laser experiments. However, for low-energy neutrons, the time length of the signal can be hundreds of  $\mu\text{s}$  or several ms. The capacitance is unable to maintain such a long-time switch and is discharged in approximately 10  $\mu\text{s}$ , though a bigger capacitance can be used to provide a large flow current output. However, the characteristics of the RC loop determine that a large capacitance inevitably leads to a slower response time. For example, to detect the epithermal neutron signal in dozens of  $\mu\text{s}$ , a capacitor over 1  $\mu\text{F}$  is needed to keep the bias applied on the gated dynodes. As the resistances between dynodes are generally hundreds of k $\Omega$ , in that case, the RC time constant can be evaluated as  $>0.1$  s. The time is obviously too slow for the neutron detection. A time-gated PMT with an ETG circuit that is normally on may be a solution for this problem. Previous research [28] has reported that switching the dynodes at the cathode end of a tube (K, Dy1 and Dy2) can result in a higher cut-off ratio and less interference on the normal response. However, for the present purpose, time-gating by switching the K bias is not feasible for the PMT due to the slow response time ( $>100$   $\mu\text{s}$ ) of the semitransparent alkali photocathode.

In this study, we developed a customized time-gated neutron TOF detector with a high cut-off ratio for the time gate, a large tolerance for the load current, and the ability to maintain linearity throughout long time measurements. The cut-off ratio refers to the

electron gain of the PMT between the on and off states, which is controlled by the ETG system. We designed a time-gated PMT with an ETG circuit that is normally on. The normally on ETG can maintain the PMT in a normal working response and shut down when there is no control pulse input and a square pulse, respectively. With this design, transient shutdowns are needed only in a very short period of several  $\mu\text{s}$  during a laser shot. The normally on ETG ensures an unlimited measuring time. The fast-switching gate and high cut-off ratio allow measurements in high-energy laser experiments with intense background and noise levels.

Furthermore, we conducted test experiments using a fast ignition experiment (LFEX) laser system at the Institute of Laser Engineering (ILE), Osaka University. We coupled the time-gated PMT with a  $^6\text{Li}$  glass scintillator to form a time-gated epithermal neutron detector. The detector was set with a neutron beamline of 1.07 m. Two neutron resonance samples, W and Ag, were placed along the beamline for the evaluation of the epithermal neutron signal via neutron resonance absorption.

## 2. Materials and Methods

### 2.1. Development of the Time-Gated PMT

The PMT we used for time-gated development is an 8-stage linear-focused type HAMAMATSU-R2083, which provides a 46 mm diameter, the effective area of a bialkali photocathode, and an anode pulse rise time of 0.7 ns. A diagram of the structure is shown in Figure 1. There is a focusing grid (G) and an accelerator electrode (ACC) between the photocathode (K) and dynodes (Dy  $n$ ,  $n = 1, 2, 3\dots$ ) to increase the collection rate and reduce the photoelectron transit time [30]. The multiplication of electrons is dominated by the voltage of the dynodes. The electrons are guided by the potential difference between the dynodes, reflected stage by stage, and finally collected to output a current signal by the anode.

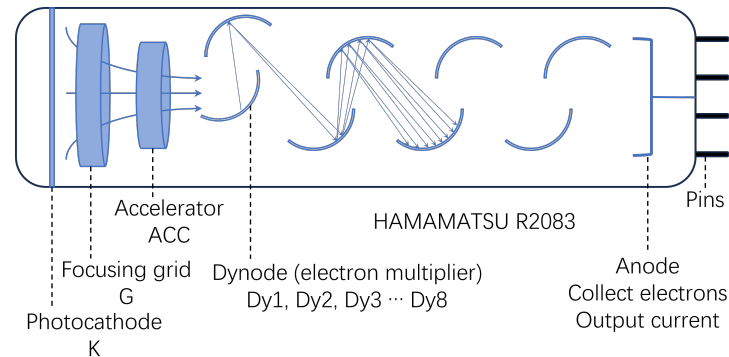
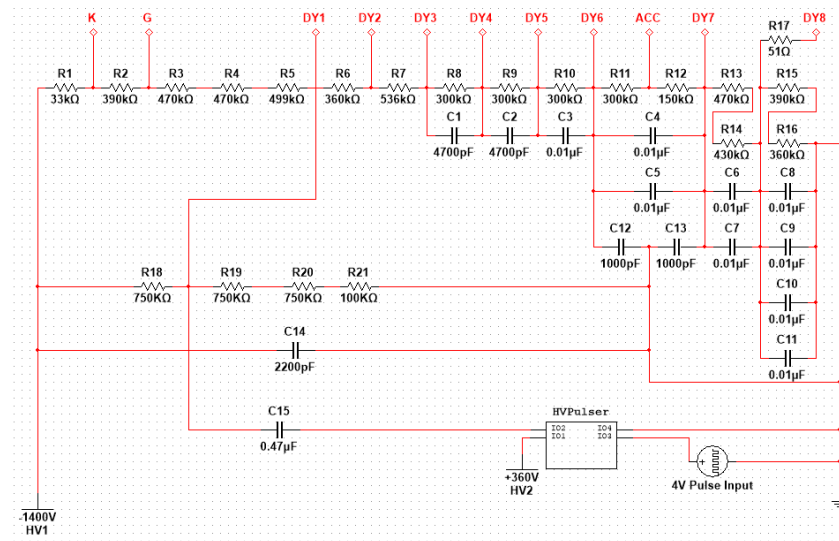
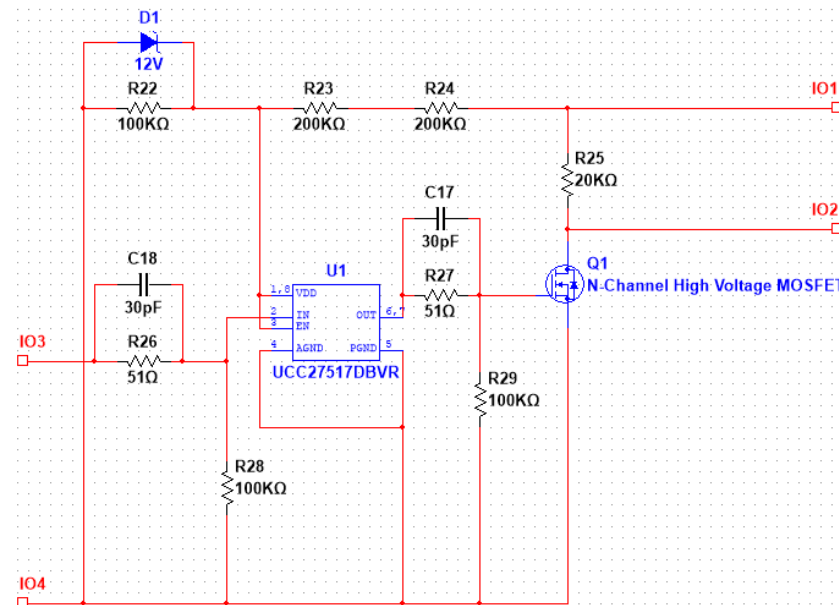


**Figure 1.** R2083 manufactured by HAMAMATSU Photonics.

To realize a normally on gate, we designed a voltage-dividing circuit for dynodes and added an ETG subcircuit on Dy1 to reverse the bias between Dy1 and Dy2 during the high-level gate-control signal. The voltage-dividing circuit and ETG subcircuit are shown in Figure 2a,b. The voltage-dividing circuit is the main circuit of the PMT and is powered by a high voltage of  $-1400$  V. Therefore, the potential of each dynode increases stage by stage from Dy1 to Dy8 to ensure that the electrons can be accelerated between the dynodes. The capacitors connected in parallel with the resistors in the last stages stabilize the voltages to maintain linearity when the large number of electrons hitting on the dynodes cause reverse currents [31]. Dy1 is connected to an independent parallel branch separately, which supplies a potential. The ETG subcircuit, which is named HV Pulser and depicted in Figure 2b, is also connected to Dy1 through capacitor C15. HV Pulser IO1-4 is connected to a  $+360$  V high-voltage power source with an output to capacitor C15, a 4 V TTL control pulse signal input, and the electrical ground. The control signal is input to a gate driver, UCC27517DBVR, which drives an N-channel high-voltage MOSFET (UF3C065080K3S) to generate a square pulse of 360 V.



(a)



(b)

**Figure 2.** (a) Main circuit of the time-gated PMT. (b) The ETG subcircuit (HV Pulsar) is connected to the main circuit (as IO1-4, corresponding to the same ports in (a)).

The expected temporal characteristic of the time-gated PMT is shown in Figure 3a. When a +4 V TTL signal is delivered to the HV Pulsar, a square pulse of +360 V is generated and delivered to Dy1 through C15. The potential of Dy1 increases by 360 V, making it 10 V higher than the potential of Dy2. Therefore, the bias between Dy1 and Dy2 is reversed to prevent the electrons from reaching Dy2. Thus, the gate is off and the gain of the PMT is theoretically close to 0. In the normal state, the Dy1 potential is lower than that of Dy2. The electrons are accelerated to Dy2, multiplied in the subsequent stages and finally output as a current signal from the anode. The temporal performance of the time-gated PMT was tested with an LED light in a darkroom, and the test results are shown in Figure 3b. The gate control signal, DC power to the LED, and PMT output signal were recorded by an oscilloscope. The gate control signal was a TTL pulse generated by a digital pulse generator (DG535), as shown by the black line. The LED light was powered by a DC pulse output of DG535, as shown by the red line. The level of the input gate control signal changed during

the period when the LED was glowing. The response signal of the time-gated PMT was recorded and is represented by the blue line. Before the gate control signal changed to a low level, although there was incident light from the LED, the response signal of the PMT was zero. When the gate control signal changed to a low level, the gain of the PMT was restored, and the response signal was output with a stable linearity. An enlarged figure of the lower edge of the gate controlling signal is shown on the left of Figure 3b. Here, we defined two parameters to evaluate the time performance of the time-gated PMT: the transit time and the raising time. The transit time represents the time from the start of the low edge of the gate signal to the start of the high edge of the gain. The rising time is the gain of the time-gated PMT from 0 to the maximum. These two delays are generated by the external capacitance in the path when the bias is passed to Dy1. The transit time and raising time were determined to be approximately 170 ns and 400 ns, respectively. In practical operation, the transit time can be offset by adjusting the gate signal time. The gain of the time-gated PMT was calibrated by a typical HAMAMATSU H2431-50 PMT module with an LED light. By comparing the output signal levels of H2431-50 and time-gated PMT, we evaluated the gain of the time-gated PMT to be  $8 \times 10^4$  during the on period.

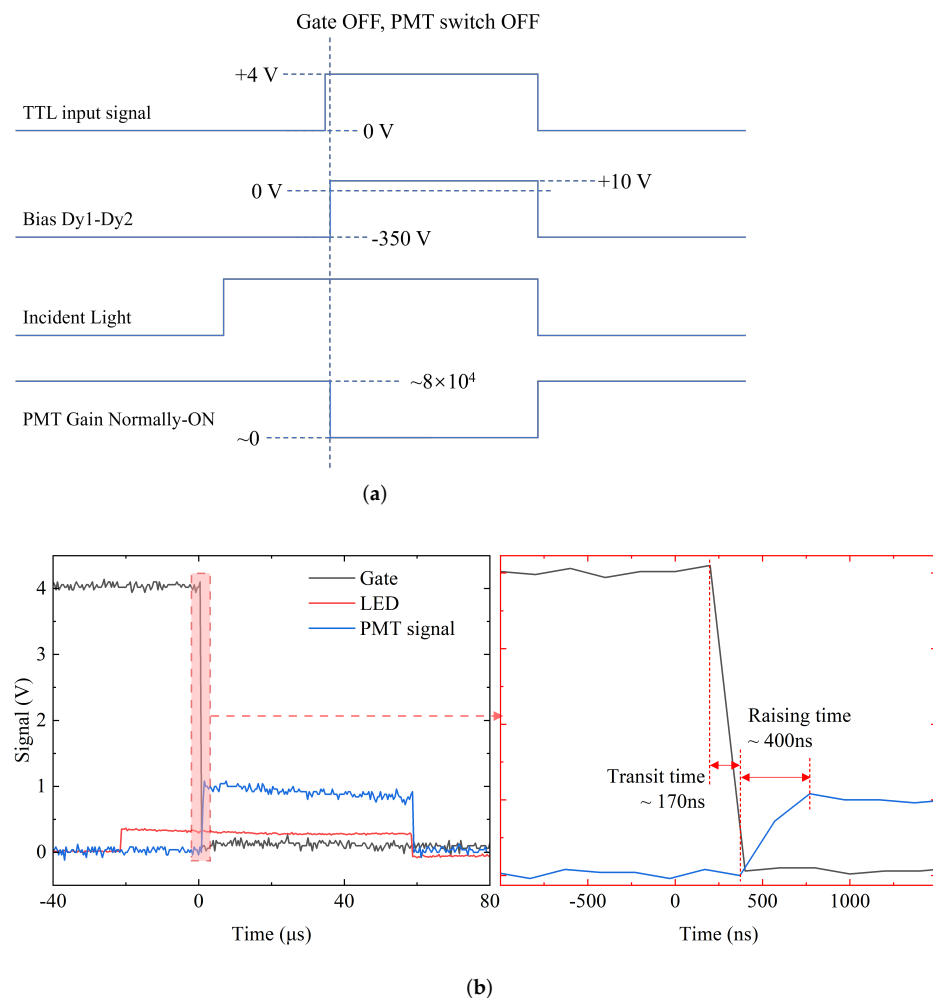


**Figure 3.** (a) Timeline of the TTL input signal, bias of Dy1-Dy2, incident light, and gain of the PMT. (b) The response test of the time-gated PMT. The black line (gate) is the TTL signal input to the ETG circuit. The red line (LED) is the voltage applied on LED. The blue line (PMT signal) is the response signal of the PMT. The translucent red region is zoomed in to the axis on the right side.

The effective time of the high-voltage pulse applied on Dy1 was determined by the time constant of the RC circuit containing C15. This design ensures an effective cut-off duration of dozens of  $\mu\text{s}$ , which is significantly longer than the pulse of intense X-rays

that generally decays in 100~200 ns. The secondary light emitted by the X-ray-excited scintillation crystals can remain for a relatively long time (a few  $\mu\text{s}$ ).

## 2.2. Experimental Demonstration Using Laser-Driven Neutrons

To verify the feasibility of the time-gated detector in high-energy laser experiments, we implemented test laser shots using LFEX. The experimental setup is shown in Figure 4. In a high-vacuum chamber ( $<10^{-5}$  Torr), the 4 laser beams of LFEX were focused on a 5  $\mu\text{m}$  thick deuterated polystyrene (CD) foil target with an intensity of  $\sim 1 \times 10^{19}$   $\text{W}\cdot\text{cm}^{-2}$ , an energy of 1300 J, and a 1.5 ps pulse duration [7]. A secondary target of cylindrical Be with high-density polyethylene (HDPE) was placed 5 mm downstream of the CD foil, resulting in the generation of fast neutrons and slower neutrons in the energy region of eV, respectively. The petawatt peak power of LFEX allows one to generate fast neutrons up to  $10^{11}$  [7,19,32], which is advantageous for the single-shot neutron analysis in the present study. The time-gated PMT was coupled with a  ${}^6\text{Li}$  glass scintillator (GS20, Scintacor Ltd., Cambridge, UK, 10 mm in thickness, 25.4 mm in radius). The neutron-induced nuclear reaction of  ${}^6\text{Li}(n,T)\alpha$  provides a large cross section in the low-energy region, which contributes to the high efficiency of neutron detection. The detection efficiency was calculated from the  ${}^6\text{Li}(n,T)\alpha$  cross-section data obtained from the JENDL4.0 database [33], considering the weight proportion and fraction of  ${}^6\text{Li}$  in the GS20 scintillator [34]. According to the calculation (Figure 5), a  ${}^6\text{Li}$  glass scintillator with a thickness of 10 mm can provide an approximately 20~90% detection efficiency in the 1~100 eV energy region. The GS20 scintillator was combined with the photosensitive interface of the PMT with a silicon optical glue. This scintillation detector was used as a neutron TOF detector at 1.07 m from the CD target. An aluminum flange (with a thickness of 2 mm) on the laser chamber was installed to provide a high transmittance of epithermal neutrons along the beamline. On the side of the detector, 5 cm thick lead and 1 mm aluminum foil were used as a shield to protect the detector from the EM shock and the background of neutron scattering.

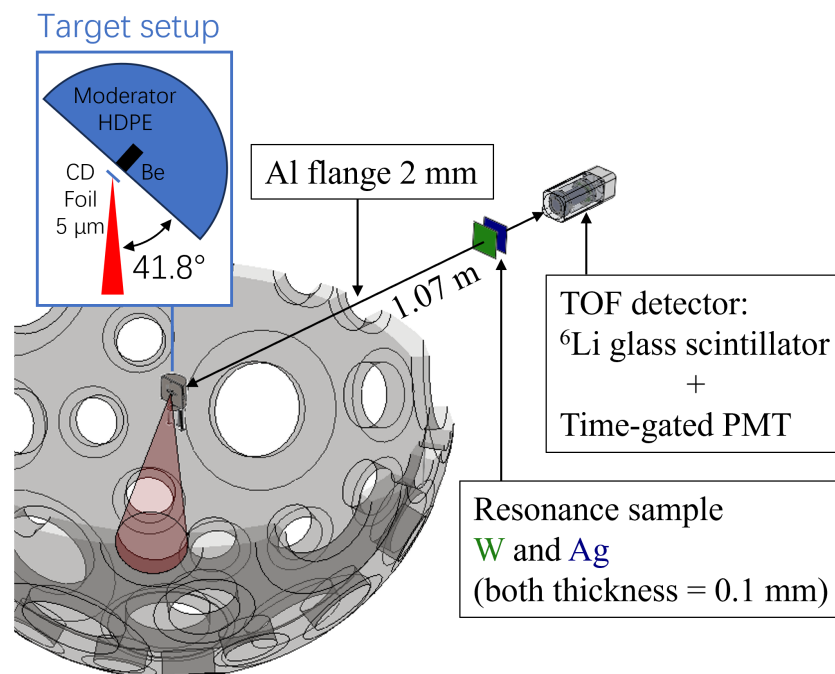


**Figure 4.** Laser-driven neutron experimental setup.

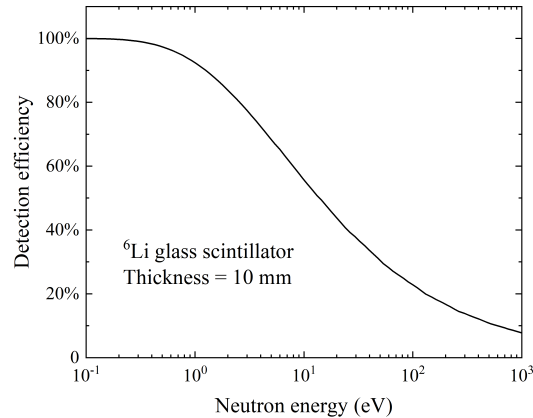


**Figure 5.** Calculated detection efficiency of 10 mm thick GS20.

### 3. Results

#### 3.1. The Evaluation of X-ray Cut-Off Ratio of the Time-Gated Detector

To evaluate the X-ray cutoff of the time-gated detector, the neutron generator and the moderator were removed for the test shots, while the rest of the setup was retained. The gate-off time window was set from 1  $\mu$ s before the laser shot to 1  $\mu$ s after the laser shot. The signal of the X-rays induced by the laser incident on the CD foil target was observed in the response signal (the enlarged part in Figure 6) regardless of the cutoff. This was attributed to the direct irradiation of the X-rays on the secondary and subsequent dynodes in the PMT. The ionization of the residual gas in the PMT further generated electrons. The direct irradiation-induced X-ray signal was acceptable when it was within the tolerance of the PMT. When the ETG system was switched on, the PMT output noise signals, including residual X-rays and scattered neutrons, as discrete pulses after 1.5  $\mu$ s (Figure 6). For epithermal neutrons with energy of hundreds of eV, the most applied scintillator  $^6\text{Li}$  glass generated approximately 6000 photons for every neutron incidence event [35]. Considering the gain of the time-gated detector, we estimated the response signal level of a neutron to be 10~100 mV. The signal level was consistent with the pulse height in the test signal (Figure 6), suggesting that some background (scattering neutrons and X-rays) was detected in the CD shots. The results of the test experiments showed an effective cutoff of the X-ray signals, while some background neutrons were detected after the gate switch was on.

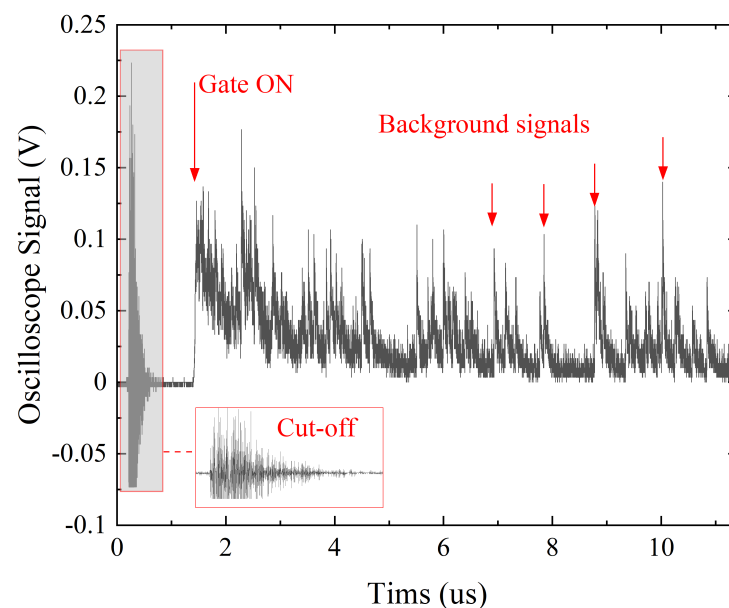


**Figure 6.** The response signal of a gated PMT in a CD shot without Be or HDPE.

### 3.2. Demonstration for Neutron Resonance Measurement

The neutron resonance absorption measurements [7] were implemented with the introduced setup (Figure 4). Two resonance absorbers (W and Ag, both of size  $100 \times 100 \times 0.1$  mm) were set in the neutron beamline, outside of the laser chamber. The time-gated detector was set to switch on  $6 \mu\text{s}$  after the laser pulse. The X-rays generated by the laser irradiation and the neutron generation were observed in the raw signal (Figure 7a) as a sharp peak at time zero. Compared to the main signals detected after the gate was switched on, the X-ray signals showed much lower amplitudes due to the cut-off of the ETG system. An intense main signal pulse with a height of several volts was observed at the time the gate was switched on. The signal showed exponential decay. This indicated that the main contribution of the pulse was the charge remaining in the PMT during the gate-off time. Two dips were observed  $30 \mu\text{s}$  after the laser shot (enlarged part in Figure 7a). As seen by converting time to energy, the energies of the dips corresponded to the neutron resonances of  $^{182}\text{W}$  at 4.15 eV and  $^{109}\text{Ag}$  at 5.19 eV. The dips in the signal demonstrated that eV-energy neutrons were successfully detected by our time-gated detector at 1.07 m. Considering the neutron cross section of Ag and Ta, the samples with a 0.1 mm thickness should absorb over 90% neutrons. However, the small dips in raw data (Figure 7a) were far less than the total signal height, which indicated the lack of statistics or an intense background. The theoretical transmittance of neutrons (dashed and dotted lines in Figure 7b) were calculated using the cross-section data obtained from the JENDL4.0 database [33]. By considering the neutron pulse broadening in the moderator, the transmittance of the neutrons was evaluated as shown in Figure 7b. Compared with the theoretical calculation, the experimental transmittance showed broader peaks, which is thought to be influenced by some background and residual emissions in  $^6\text{Li}$  glass.

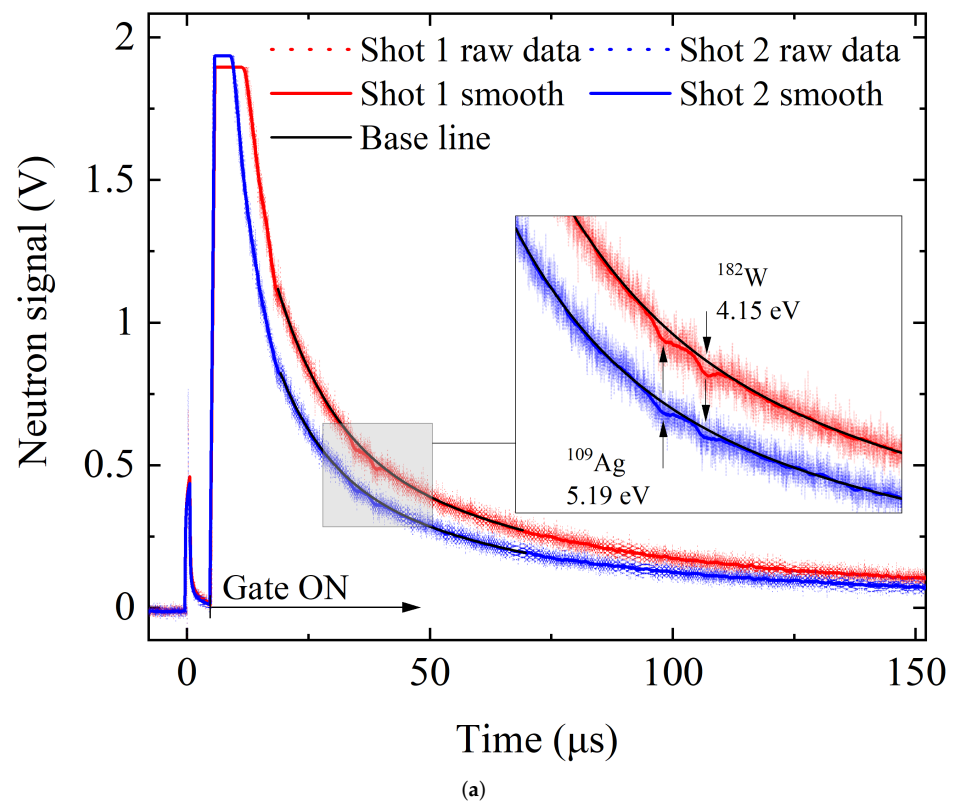
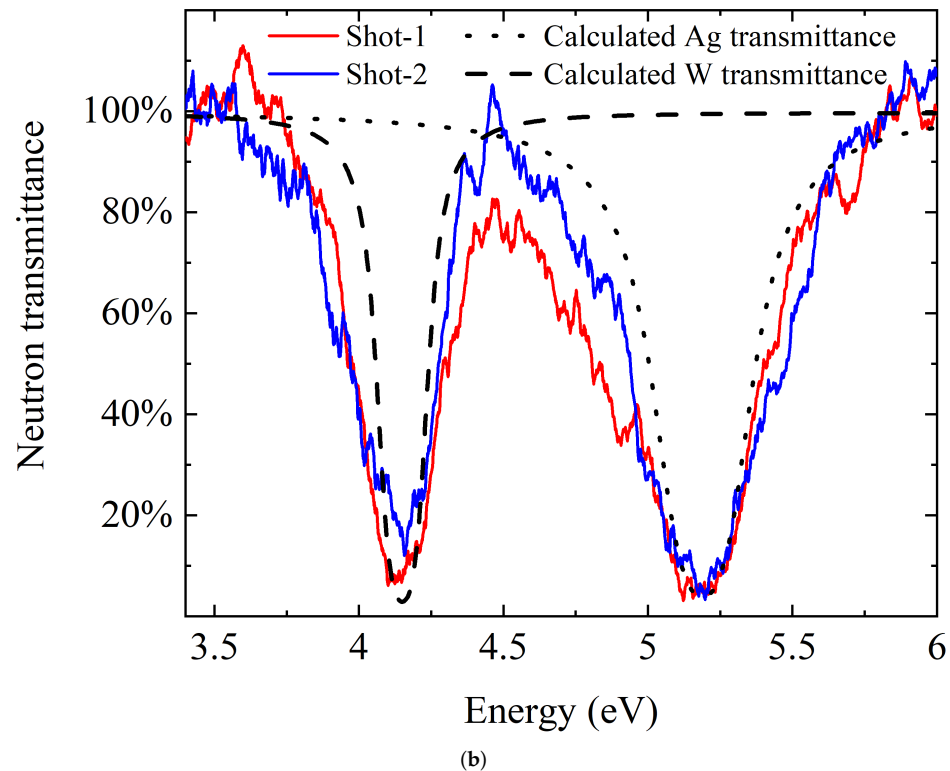


Figure 7. Cont.



**Figure 7.** (a) The epithermal neutron signals. Each of the signals was recorded after a single shot of the laser. The neutron resonance absorption values of  $^{109}\text{Ag}$  at 5.19 eV and  $^{182}\text{W}$  at 4.15 eV were observed in the signals. Baselines were fitted for the signals to determine the amplitude of the neutron resonance absorption. (b) The neutron transmittance results were analyzed in terms of the raw signals. The theoretical transmittance of the experimental samples was calculated from the cross-section data obtained from the JENDL4.0 database [33].

#### 4. Discussion

The design of the ETG system introduced in this paper has high flexibility and development potential to be used in various high-power laser experimental conditions. For example, the RC loop that transmits the bias voltage generated by the ETG system can be further developed. The RC time constant determines the transient time of the circuit, which is the gate-off time in a normally on PMT. Since laser beams have a very short pulse and the X-ray backgrounds rapidly decay within hundreds of ns, the gate-off time can be set to very short. Therefore, the small RC can realize an ultrafast ETG for the beamline shorter than 1 m or higher neutron energies (KeV~MeV). The shorter beamline in laser-driven neutron experiments significantly improves the detecting efficiency of neutrons. With the development of LDNSs, the time-gated detector can be used to configure a neutron spectroscopy system for multiple purposes as introduced in Section 1. However, the experimental results above showed small peaks that could be unclear for further investigations. The results reported in Ref. [7] showed single-shot resonance measurements which were detected by the same time-gated PMT with a slight change in the switching speed. Furthermore, similar ETG circuits can be connected to multiple dynodes to provide a higher cut-off ratio.

In our experimental results (Figure 7), the backgrounds still existed after the gate-on time. As an alternative approach to avoid these backgrounds, Ref. [36] reported a method in which the optical detector was set far from the scintillator to avoid the X-rays. Only the neutron scintillator was set in the beamline, and a light guide was used to transmit the light signal to the optical detector. This method seriously reduced the detection efficiency of neutrons but had a good shielding effect on backgrounds such as X-rays and scattered neutrons. The time-gated detector could integrate that method to improve the quality of

the resonance spectrum. In addition, since there was no shield and collimator along the beamline in our detector test experiments, a neutron collimator could be expected to keep neutron beams clear from the backgrounds.

## 5. Conclusions

We designed a time-gated PMT with a normally on ETG circuit. The time-gated PMT was coupled with a  $^6\text{Li}$  glass scintillator for a TOF epithermal neutron detector used in high-energy laser experiments. The ETG was tested with an LED light, showing a raising time of  $\sim 400$  ns and a stable linearity within the gate-on time. A neutron resonance absorption measurement experiment was conducted using an LFEX laser system at ILE, Osaka Univ. The time-gated detector was set at 1.07 m from the main target. The ETG circuit showed a high cutoff on X-rays generated from the laser shot time. The neutron resonance absorption values of  $^{109}\text{Ag}$  at 5.19 eV and  $^{182}\text{W}$  at 4.15 eV were detected. The neutron signal level and the transmittance of neutrons were evaluated. The experimental results demonstrated that our design was suitable for epithermal neutron detection with a short distance in high-energy laser experiments. The normally on ETG circuit achieved a stable linear response with an infinitely long time after the gate was switched on. The ETG circuit is expected to be applicable for any PMT with general voltage-dividing circuits. Minor modifications are possible for the ETG circuit to adapt to practical applications.

**Author Contributions:** Conceptualization, A.Y. and Z.L.; methodology, Z.L., Y.A. (Yuki Abe) and Y.A. (Yasunobu Arikawa); formal analysis, Z.L. and T.W.; data collection and analysis, Z.L.; writing—original draft preparation, Z.L.; writing—review and editing, A.Y., T.H., Y.A. (Yasunobu Arikawa), A.M. and S.R.M.; supervision, A.Y. and T.H.; project administration, A.Y.; funding acquisition, A.Y. All authors have read and agreed to the published version of the manuscript.

**Funding:** This work was funded by a JSPS KAKENHI Grant-in-Aid for Scientific Research (JP22H02007, JP22H01239), JST A-STEP (AS2721002c), and JST PRESTO (JPMJPR15PD). Zechen Lan was supported by a JSPS Research Fellowship for Young Scientists DC2 (202311207). Zechen Lan (before Apr. 2023) and Tianyun Wei were supported by JST SPRING, grant number JPMJSP2138.

**Informed Consent Statement:** Not applicable.

**Data Availability Statement:** The data presented in this study are available on request to the corresponding author.

**Acknowledgments:** The authors thank the technical support staff at ILE for their assistance with the laser operation, target fabrication, and plasma diagnostics. This work was supported by the Collaboration Research Program of ILE, Osaka University.

**Conflicts of Interest:** Seyed Reza Mirfayzi was employed by the company Tokamak Energy Ltd. The remaining authors declare that the research was conducted in the absence of any commercial or financial relationships that could be construed as a potential conflict of interest.

## Abbreviations

The following abbreviations are used in this manuscript:

LDNS	Laser-driven neutron source
PMT	Photomultiplier tube
TOF	Time-of-flight
ETG	Electrical time-gating
HDPE	High-density polyethylene

## References

1. Groeger, S.; Bison, G.; Knowles, P.E.; Wynands, R.; Weis, A. Laser-pumped cesium magnetometers for high-resolution medical and fundamental research. *Sens. Actuators A Phys.* **2006**, *129*, 1–5. [[CrossRef](#)]
2. Yuan, V.; Bowman, J.D.; Funk, D.; Morgan, G.; Rabie, R.; Ragan, C.; Quintana, J.; Stacy, H. Shock temperature measurement using neutron resonance spectroscopy. *Phys. Rev. Lett.* **2005**, *94*, 125504. [[CrossRef](#)] [[PubMed](#)]

3. Higginson, D.; McNaney, J.; Swift, D.; Bartal, T.; Hey, D.; Kodama, R.; Le Pape, S.; Mackinnon, A.; Mariscal, D.; Nakamura, H.; et al. Laser generated neutron source for neutron resonance spectroscopy. *Phys. Plasmas* **2010**, *17*, 100701. [[CrossRef](#)]
4. Mirani, F.; Maffini, A.; Passoni, M. Laser-driven neutron generation with near-critical targets and application to materials characterization. *Phys. Rev. Appl.* **2023**, *19*, 044020. [[CrossRef](#)]
5. Brenner, C.; Mirfayzi, S.; Rusby, D.; Armstrong, C.; Alejo, A.; Wilson, L.; Clarke, R.; Ahmed, H.; Butler, N.; Haddock, D.; et al. Laser-driven x-ray and neutron source development for industrial applications of plasma accelerators. *Plasma Phys. Control. Fusion* **2015**, *58*, 014039. [[CrossRef](#)]
6. Lancaster, K.; Karsch, S.; Habara, H.; Beg, F.; Clark, E.; Freeman, R.; Key, M.; King, J.; Kodama, R.; Krushelnick, K.; et al. Characterization of  ${}^7\text{Li}(p,n){}^7\text{Be}$  neutron yields from laser produced ion beams for fast neutron radiography. *Phys. Plasmas* **2004**, *11*, 3404–3408. [[CrossRef](#)]
7. Yogo, A.; Lan, Z.; Arikawa, Y.; Abe, Y.; Mirfayzi, S.; Wei, T.; Mori, T.; Golovin, D.; Hayakawa, T.; Iwata, N.; et al. Laser-driven neutron generation realizing single-shot resonance spectroscopy. *Phys. Rev. X* **2023**, *13*, 011011. [[CrossRef](#)]
8. Alejo, A.; Krygier, A.; Ahmed, H.; Morrison, J.; Clarke, R.; Fuchs, J.; Green, A.; Green, J.; Jung, D.; Kleinschmidt, A.; et al. High flux, beamed neutron sources employing deuteron-rich ion beams from D2O-ice layered targets. *Plasma Phys. Control. Fusion* **2017**, *59*, 064004. [[CrossRef](#)]
9. Günther, M.; Rosmej, O.; Tavana, P.; Gyrdymov, M.; Skobliakov, A.; Kantsyrev, A.; Zähler, S.; Borisenko, N.; Pukhov, A.; Andreev, N. Forward-looking insights in laser-generated ultra-intense  $\gamma$ -ray and neutron sources for nuclear application and science. *Nat. Commun.* **2022**, *13*, 170. [[CrossRef](#)]
10. Arikawa, Y.; Morace, A.; Abe, Y.; Iwata, N.; Sentoku, Y.; Yogo, A.; Matsuo, K.; Nakai, M.; Nagatomo, H.; Mima, K.; et al. Demonstration of efficient relativistic electron acceleration by surface plasmonics with sequential target processing using high repetition lasers. *Phys. Rev. Res.* **2023**, *5*, 013062. [[CrossRef](#)]
11. Clark, E.; Krushelnick, K.; Zepf, M.; Beg, F.; Tatarakis, M.; Machacek, A.; Santala, M.; Watts, I.; Norreys, P.; Dangor, A. Energetic heavy-ion and proton generation from ultraintense laser-plasma interactions with solids. *Phys. Rev. Lett.* **2000**, *85*, 1654. [[CrossRef](#)] [[PubMed](#)]
12. Maksimchuk, A.; Gu, S.; Flippo, K.; Umstadter, D.; Bychenkov, V.Y. Forward ion acceleration in thin films driven by a high-intensity laser. *Phys. Rev. Lett.* **2000**, *84*, 4108. [[CrossRef](#)] [[PubMed](#)]
13. Snavely, R.; Key, M.; Hatchett, S.; Cowan, T.; Roth, M.; Phillips, T.; Stoyer, M.; Henry, E.; Sangster, T.; Singh, M.; et al. Intense high-energy proton beams from petawatt-laser irradiation of solids. *Phys. Rev. Lett.* **2000**, *85*, 2945. [[CrossRef](#)]
14. Passoni, M.; Bertagna, L.; Zani, A. Target normal sheath acceleration: Theory, comparison with experiments and future perspectives. *New J. Phys.* **2010**, *12*, 045012. [[CrossRef](#)]
15. Yogo, A.; Mima, K.; Iwata, N.; Tosaki, S.; Morace, A.; Arikawa, Y.; Fujioka, S.; Johzaki, T.; Sentoku, Y.; Nishimura, H.; et al. Boosting laser-ion acceleration with multi-picosecond pulses. *Sci. Rep.* **2017**, *7*, 42451. [[CrossRef](#)] [[PubMed](#)]
16. Macchi, A.; Borghesi, M.; Passoni, M. Ion acceleration by superintense laser-plasma interaction. *Rev. Mod. Phys.* **2013**, *85*, 751. [[CrossRef](#)]
17. Roth, M.; Jung, D.; Falk, K.; Guler, N.; Deppert, O.; Devlin, M.; Favalli, A.; Fernandez, J.; Gautier, D.; Geissel, M.; et al. Bright laser-driven neutron source based on the relativistic transparency of solids. *Phys. Rev. Lett.* **2013**, *110*, 044802. [[CrossRef](#)]
18. Kleinschmidt, A.; Bagnoud, V.; Deppert, O.; Favalli, A.; Frydrych, S.; Hornung, J.; Jahn, D.; Schaumann, G.; Tebartz, A.; Wagner, F.; et al. Intense, directed neutron beams from a laser-driven neutron source at PHELIX. *Phys. Plasmas* **2018**, *25*, 053101. [[CrossRef](#)]
19. Mirfayzi, S.; Yogo, A.; Lan, Z.; Ishimoto, T.; Iwamoto, A.; Nagata, M.; Nakai, M.; Arikawa, Y.; Abe, Y.; Golovin, D.; et al. Proof-of-principle experiment for laser-driven cold neutron source. *Sci. Rep.* **2020**, *10*, 20157. [[CrossRef](#)]
20. Zimmer, M.; Scheuren, S.; Kleinschmidt, A.; Mitura, N.; Tebartz, A.; Schaumann, G.; Abel, T.; Ebert, T.; Hesse, M.; Zähler, S.; et al. Demonstration of non-destructive and isotope-sensitive material analysis using a short-pulsed laser-driven epi-thermal neutron source. *Nat. Commun.* **2022**, *13*, 1173. [[CrossRef](#)]
21. Copley, J.R.; Udovic, T.J. Neutron time-of-flight spectroscopy. *J. Res. Natl. Inst. Stand. Technol.* **1993**, *98*, 71. [[CrossRef](#)] [[PubMed](#)]
22. Kar, S.; Green, A.; Ahmed, H.; Alejo, A.; Robinson, A.; Cerchez, M.; Clarke, R.; Doria, D.; Dorkings, S.; Fernandez, J.; et al. Beamed neutron emission driven by laser accelerated light ions. *New J. Phys.* **2016**, *18*, 053002. [[CrossRef](#)]
23. Bencardino, R.; Eberhardt, J.E. Development of a fast-neutron detector with silicon photomultiplier readout. *IEEE Trans. Nucl. Sci.* **2009**, *56*, 1129–1134. [[CrossRef](#)]
24. Roecker, C.; Bernstein, A.; Bowden, N.; Cabrera-Palmer, B.; Dazeley, S.; Gerling, M.; Marleau, P.; Sweany, M.; Vetter, K. Design of a transportable high efficiency fast neutron spectrometer. *Nucl. Instrum. Methods Phys. Res. Sect. A Accel. Spectrom. Detect. Assoc. Equip.* **2016**, *826*, 21–30. [[CrossRef](#)]
25. Abe, Y.; Nakajima, N.; Sakaguchi, Y.; Arikawa, Y.; Mirfayzi, S.; Fujioka, S.; Taguchi, T.; Mima, K.; Yogo, A.; Nishimura, H.; et al. A multichannel gated neutron detector with reduced afterpulse for low-yield neutron measurements in intense hard X-ray backgrounds. *Rev. Sci. Instrum.* **2018**, *89*, 10I114. [[CrossRef](#)] [[PubMed](#)]
26. Bennett, R.; Schwenker, R. Performance of a Pulsed 6292 Photomultiplier. *Rev. Sci. Instrum.* **1959**, *30*, 836–837. [[CrossRef](#)]
27. De Martini, F.; Wacks, K.P. Photomultiplier Gate for Stimulated-Spontaneous Light Scattering Discrimination. *Rev. Sci. Instrum.* **1967**, *38*, 866–868. [[CrossRef](#)]
28. De Marco, F.; Penco, E. Pulsed photomultipliers. *Rev. Sci. Instrum.* **1969**, *40*, 1158–1160. [[CrossRef](#)]
29. Schulman, M.B. Gating circuit for linear-focused photomultiplier. *Rev. Sci. Instrum.* **1989**, *60*, 1264–1266. [[CrossRef](#)]

30. Lee, S.; Lee, M.S.; Won, J.Y.; Lee, J.S. Performance of a new accelerating-electrode-equipped fast-time-response PMT coupled with fast LGSO. *Phys. Med. Biol.* **2018**, *63*, 05NT03. [[CrossRef](#)]
31. Bristow, M.P.; Bundy, D.H.; Wright, A.G. Signal linearity, gain stability, and gating in photomultipliers: Application to differential absorption lidars. *Appl. Opt.* **1995**, *34*, 4437–4452. [[CrossRef](#)]
32. Yogo, A.; Mirfayzi, S.R.; Arikawa, Y.; Abe, Y.; Wei, T.; Mori, T.; Lan, Z.; Hoonoki, Y.; Golovin, D.O.; Koga, K.; et al. Single shot radiography by a bright source of laser-driven thermal neutrons and X-rays. *Appl. Phys. Express* **2021**, *14*, 106001. [[CrossRef](#)]
33. Shibata, K.; Iwamoto, O.; Nakagawa, T.; Iwamoto, N.; Ichihara, A.; Kunieda, S.; Chiba, S.; Furutaka, K.; Otuka, N.; Ohsawa, T.; et al. JENDL-4.0: A new library for nuclear science and engineering. *J. Nucl. Sci. Technol.* **2011**, *48*, 1–30. [[CrossRef](#)]
34. Tyrrell, G.C. Phosphors and scintillators in radiation imaging detectors. *Nucl. Instrum. Methods Phys. Res. Sect. A Accel. Spectrom. Detect. Assoc. Equip.* **2005**, *546*, 180–187. [[CrossRef](#)]
35. Kawaguchi, N.; Yanagida, T.; Novoselov, A.; Kim, K.J.; Fukuda, K.; Yoshikawa, A.; Miyake, M.; Baba, M. Neutron responses of Eu<sup>2+</sup> activated LiCaAlF<sub>6</sub> scintillator. In Proceedings of the IEEE Nuclear Science Symposium Conference Record, Dresden, Germany, 19–25 October 2008; pp. 1174–1176.
36. Kishon, I.; Kleinschmidt, A.; Schanz, V.; Tebartz, A.; Noam, O.; Fernandez, J.; Gautier, D.; Johnson, R.; Shimada, T.; Wurden, G.; et al. Laser based neutron spectroscopy. *Nucl. Instrum. Methods Phys. Res. Sect. A Accel. Spectrom. Detect. Assoc. Equip.* **2019**, *932*, 27–30. [[CrossRef](#)]

**Disclaimer/Publisher’s Note:** The statements, opinions and data contained in all publications are solely those of the individual author(s) and contributor(s) and not of MDPI and/or the editor(s). MDPI and/or the editor(s) disclaim responsibility for any injury to people or property resulting from any ideas, methods, instructions or products referred to in the content.